ADVANCED FUNCTIONAL MATERIALS
www.afm-journal.de

Quantum Dot–Carbon Nanotube Hybrid Phototransistor with an Enhanced Optical Stark Effect

Chandan Biswas, Hyun Jeong, Mun Seok Jeong, Woo Jong Yu, Didier Pribat, and Young Hee Lee**

Enhanced carrier–carrier interactions in hybrid nanostructures exhibit exceptional electronic and optoelectronic properties. Carbon nanotubes demonstrate excellent switching behavior with high on/off ratio and high mobility but do not show photoresponse in the visible range, whereas quantum dots (QDs) shows excellent optical response in various optical ranges which can be tuned with diameter. Here, a simple and effective way to develop hybrid phototransistors with extraordinary optoelectronic properties is presented by decorating semiconducting QDs on the surface of a single-walled carbon nanotube (SWCNT). This hybrid structure demonstrates clear negative photoresponse and optical switching behavior, which could be further tuned by applying external gate bias in the future. A clear type conversion of SWCNT transistor from p-type to n-type caused by a charge transfer from attached QDs to CNT is demonstrated. Moreover, this hybrid structure also demonstrates an enhancement in 'optical Stark effect' without applying any external electric field. Charged SWCNT surface plays a key role behind the enhancement of optical Stark effect in QDs. The carrier dynamics of the QD and CNT heterostructures system highlights the potential application opportunity of the quantum dot systems, which can be adaptable to the current technologies.

1. Introduction

Strong spatial confinement of electronic wave functions[1] in semiconducting quantum dots (QDs) enhances carrier-carrier interactions, which lead to numerous exotic electronic and optoelectronic properties significantly different from their bulk counterparts. Exciton (or carrier) multiplication,[2–4] Stark effect,[5–8] and band shifting[9,10] are among the key features of QDs and are strongly dependent on the shape, size, and architecture, in contrast to their bulk counterparts. Photodetectors with ultrahigh sensitivity can be implemented exploiting enhanced carrier interactions in semiconducting QDs by attaching to an efficient photogenerated charge carriers. Multiple carrier generation by single photon excitation is the key to achieve highly efficient photodetectors. Previously investigated efficient photomultipliers and avalanche photodiodes operate under high applied voltage and incompatible with current embedded circuit technologies (such as metal-oxide semiconductor systems).[11,12] Phototransistor is an alternative photodetector which was reported to provide high sensitivity and fabricated using III–V QDs in a two-dimensional electron gas (2DEG) systems. However, these devices were operated at very low temperature (4 K), making them unsuitable for practical applications.[13] Heterojunction phototransistors based on epitaxially grown III–V semiconductors have also been reported with high gain but the device performance significantly relies on the synthesis process, making it difficult to be compatible with existing metal-oxide semiconductor (CMOS) technologies.[14] Recently, a hybrid phototransistor was reported using semiconducting QDs and graphene with very high gain, however, the very low band gap of graphene enhances photogenerated charge recombination and limits carrier collections.[15] High energy charge carriers are often generated in QDs due to the enhanced carrier interaction by external photon excitation.[16] Energy conversion devices such as solar cells, photodetectors, and optical switching devices require carriers to be extracted from the QDs to external circuits. However, charge collectors (metals or QD assemblies)

Dr. C. Biswas[+]
WCU Department of Energy Science
Sungkyunkwan University
Suwon 440-746, Republic of Korea
Dr. H. Jeong, Dr. M. S. Jeong, Prof. Y. H. Lee
Center for Integrated Nanostructure Physics
Institute of Basic Science
WCU Department of Energy Science
Sungkyunkwan University
Suwon 440-746, Republic of Korea
E-mail: mjeong@gist.ac.kr; leeyoung@skku.edu
Dr. W. J. Yu
Department of Electronic and Electrical Engineering
Sungkyunkwan University
Suwon 440-746, Republic of Korea
Prof. D. Pribat
WCU Department of Energy Science
Sungkyunkwan University
Suwon 440-746, Republic of Korea
[+] Present address: Device Research Lab, Department of Electrical Engineering, University of California, Los Angeles, CA 90095, USA

DOI: 10.1002/adfm.201203469

hybridized with QDs reduce the carrier interactions within QDs or with metals.[3,17] A better strategy for QD-related hybrid structures is required to facilitate all these features without degradation. Exploitation of the photogenerated carriers in QDs in practical applications cannot be realized unless a new approach of charge extraction can be developed.

Low-dimensional carbon allotropes such as semiconducting single-walled carbon nanotubes (SWCNTs) and graphene exhibit exotic electrical and optoelectronic properties.[18–22] Charged SWCNT surface can be used as the anchoring base to collect photogenerated charge carriers from highly photoactive semiconducting QDs. Charged SWCNTs with high electrical mobility and tunable direct band gap material could act as highly efficient charge carriers. Moreover, accumulated charges on SWCNT surface could enhance local electric filed on QDs which could further enhance carrier-carrier interaction in QD system. Therefore, charged SWCNT expect to invoke enhancement of optical and/or electrical properties in QD system itself. Previous demonstrations focused mostly on hybridization of SWCNTs with QDs systems.[23–27] However, clear and detail demonstration of carrier extraction processes, photogenerated carrier transportation, and enhancement in optoelectronic properties in QD system due to the attachments of the charged SWCNTs has been lacking.[28]

Here, by attaching CdSe–ZnS core–shell QDs to a p-type SWCNT surface, we report a hybrid phototransistor which exhibits negative photoresponse and enhanced optical Stark effect. Clear type conversion of CNT transistor from p-type to n-type was caused by a charge transfer from QD to CNT. The decoration of negatively charged QDs (octadecylamine functional group dispersed in toluene solution) was facilitated by electrodeposition using a step potential to a positively charged SWCNT transistor. The abundance of attached QD density on CNT transistor was observed minimal near the middle of the channel compared to the electrode contact regions, which were verified by using photoluminescence (PL) intensity mapping. This hybrid phototransistor exhibits a sharp electrical photoresponse up to 86% under a broad spectral excitation (AM 1.5) and could be tunable by applying voltages. One advantage of our hybrid device is that the photoresponse efficiency could be tunable depending upon the desired value by controlling applying bias. This could be beneficial for the practical implementation of a tunable photodetector to be compatible with external circuitry.

Asymmetric changes in electron and hole wave functions and electron-hole overlap integral under an external electric field in a quantum confined structure results in the Stark effect.[29–33] The discrete energy levels of quantum dots (confined in low dimension) and their transition energy shift under an external electric field result in a quantum confined Stark effect (QCSE).[29,30] Transition energies can be also shifted by light excitations in a quantum confined QD system resulting in optical Stark effect (OSE).[8,31–33] Local charges present near the QDs create a local electric field, which results in a photoluminescence (PL) peak shift and broadening. Thus, the optical Stark effect can be monitored using PL measurements.[8] In addition to the negative photoresponse, an enhancement in the optical Stark effect was also observed due to the presence of strongly charged SWCNTs. This was verified by temporal PL peak shift and peak broadening. Accumulated charges on SWCNT surface could enhance local electric filed on QDs which could further enhance carrier–carrier interaction in QD system and results enhanced optical Stark effect.

2. Results and Discussion

Photoexited charge carrier collection from QDs to SWCNTs was facilitated by attaching CdSe–ZnS core–shell QDs to a SWCNT field effect transistor (SWCNT-FET) device. Electrodeposition technique was carried out using a SWCNT-FET device immersed in octadecylamine-functionalized QDs dispersed in toluene solution, in order to verify QD attachments on SWCNT surface (**Figure 1**a). A step potential was applied (from 1 to 6 V with 1 V step) between source-drain Ti/Au electrodes of SWCNT-FET device without gate biasing.[27] Figure 1a represents in situ source-drain current measurements with electrodeposition time. The current increased gradually as the step potential was elevated with time in SWCNT-FET device immersed in toluene solution. However, the current increased abruptly in SWCNT-FET device immersed in QD+toluene solution when the potential was elevated. In this case, the current shows a sharp peak initially at every applied step potential, followed by a gradual decrease to the current level of SWCNT in toluene at a later time. These instantaneous current peaks in SWCNT-FET immersed in QD+toluene solution could be caused by the charge transfer from the attached QDs to the SWCNT surface. The strong electrostatic attraction induces the QDs to attach to the CNT surface (Figure 1b). No appreciable accumulation of QDs was observed without applying bias. Two-dimensional mapping of photoluminescence (Figure 1c) was performed by UV laser scanning confocal microscopy to verify the spatial distribution of the QD attachment on the SWCNT surface. QDs were found to be attached not only to the SWCNT (bright region at the right of Figure 1c) surface but also to the edge of the metal electrodes. However, the QD concentration on the CNT was much higher than that of the electrodes, resulting in higher PL intensity near the CNT.

High resolution PL spectra (**Figure 2**a) were measured to investigate the QD coverage on CNT channel along its longitudinal direction. PL spectra of nine different spots (black dashed line in Figure 2b) on the CNT-FET channel starting from source electrode to drain electrode (yellow dot-dashed lines) were measured for comparison. The PL intensity profile at nine different spots along the CNT shows a maximum at both ends of the CNT channel, whereas it shows a minimum in the middle of the CNT channel (Figure 2a inset). This proves that the QDs are accumulated more abundantly near the CNT-electrode contacts due to the strong local electric field applied during electrodeposition. However, the peak position remained constant at 472 nm (2.62 eV) in QDs-attached SWCNT (QD+SWCNT Figure 2a). In addition, PL spectra of only QDs with different concentrations on SiO_2 substrate (away from CNT and metal electrodes, see Figure 2c) to confirm the PL intensity variations with different QD density. Figure 2c inset shows the PL intensity mapping obtained from the QDs on a SiO_2/Si substrate located remotely from the CNT channels and electrodes. PL spectra of three different points (X, Y, Z) with different QD

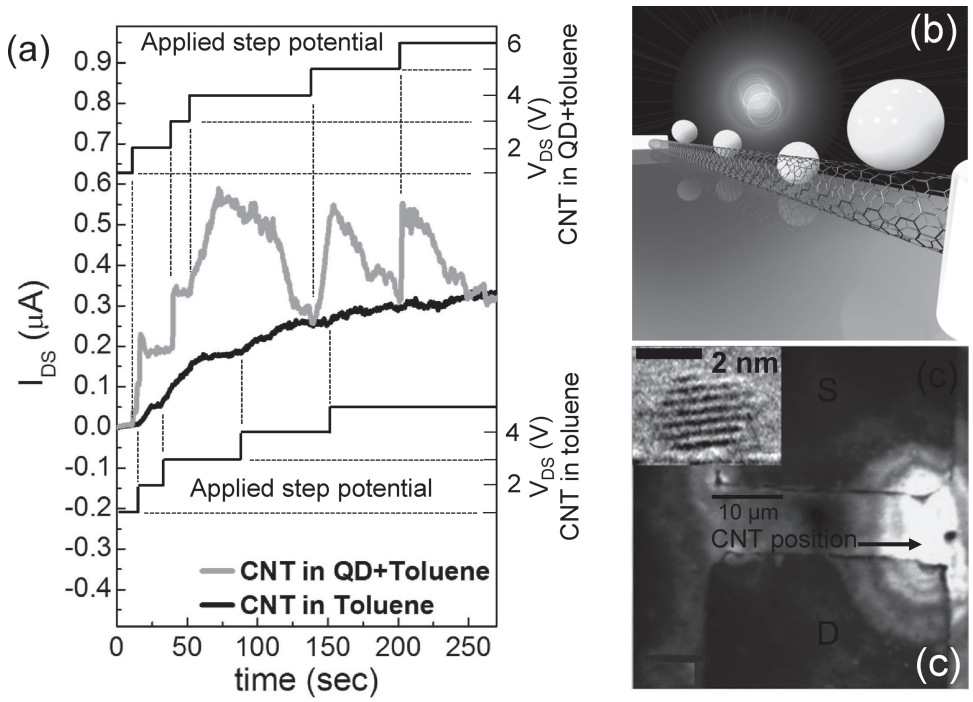

Figure 1. a) Transient source-drain current measurements of SWCNT-FET device immersed in QD+touene and toluene solution. Step potential was applied to the device immersed in QD+toluene and toluene solution, shown in the top and bottom portion of the figure, respectively (right Y axis). b) Schematic diagram of the QD-decorated CNT device. c) PL intensity profile near the CNT bridged between the source (S) and drain (D) at 482 nm (excitation wavelength: 375 nm). The inset shows the transmission electron microscopy image of the QDs attached to the carbon nanotube surface.

densities were shown in Figure 2d. The peak positions were observed consistently at 482 nm (2.57 eV). The absorption edge of QDs dispersed in toluene solution was observed at 460 nm (2.69 eV). The blue shift in the PL peak in QD+CNT samples compared to PL peak in QD samples could be related to the charge transfer from QD to the CNT, which will be discussed in the next paragraph.

The pristine SWCNT-FET showed typical p-type behavior with an on/off ratio of ≈100 and a threshold voltage (V_{th}, gate voltage axis intercept with extrapolated second derivative of I_{DS}–V_{GS} curve) of approximately +5 V (**Figure 3**a). The p-type behavior was still retained, whereas the source-drain current (I_{DS}) was reduced by around 30% (Figure 3b) in the case of QDs deposited by a simple drop of QD solution without applying a source-drain bias. On the other hand, the *I*–*V* curves of electrodeposited QD sample (described in the experimental) show a clear demonstration of type conversion from p-type to n-type (Figure 3c) with a dramatic shift in the V_{th} to the negative

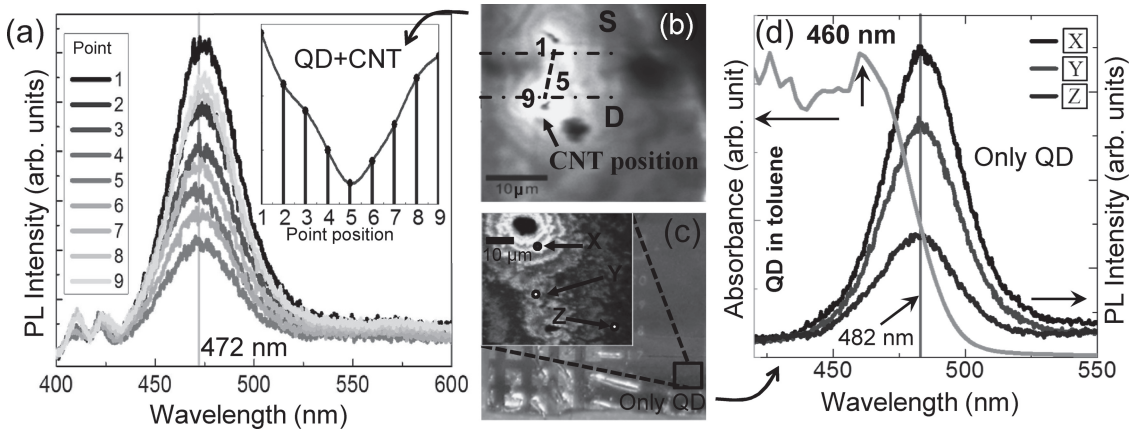

Figure 2. a) The PL spectra (measured at the position marked by number 1-9 in b) and intensity profile (inset) of the QD attached CNT connected between the two electrodes. b) Spatial PL intensity mapping from QDs on/near the CNT channel between the source and drain electrode (excitation of 375 nm). c) Optical image and PL intensity mapping of the QDs (inset) on a silica substrate located away for CNT-FET and metal electrodes (excitation energy: 375 nm). d) Absorbance of the QD dispersed in toluene solution and PL spectra obtained from three different spots (X, Y, Z in the inset of (c)) of the QDs located away from the CNT channels.

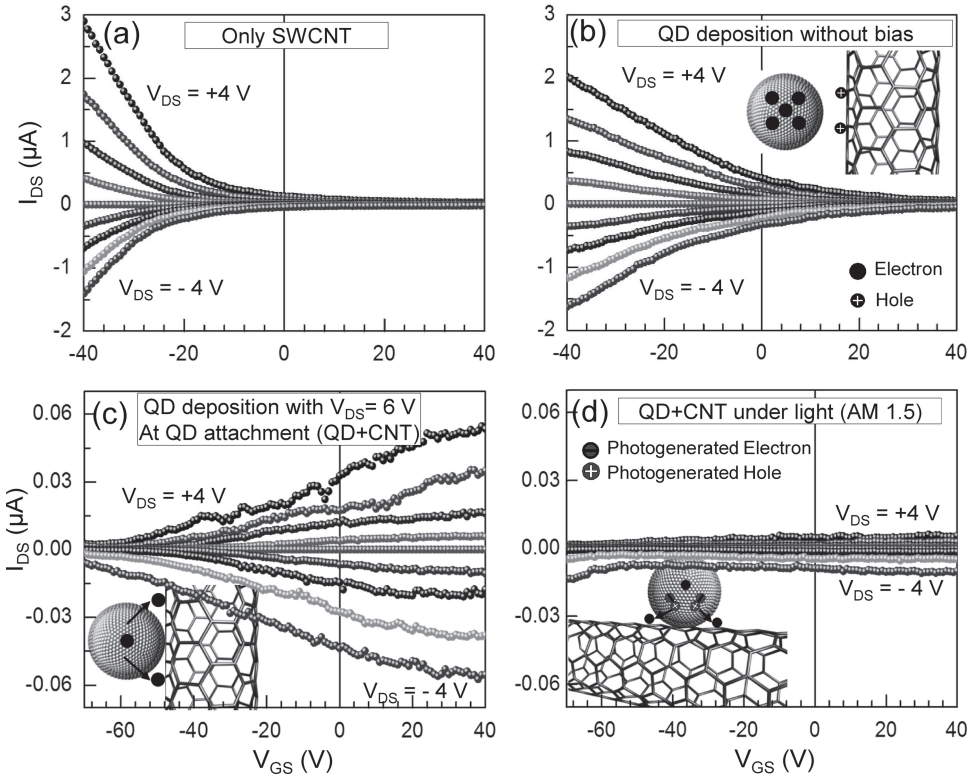

Figure 3. Transfer characteristics of the pristine SWCNT-FET a) without QD attachment, b) with one drop of QD solution and dried under vacuum for 2 h at 150 °C, c) with electrodeposited QDs on SWCNT-FET and dried under vacuum for 2 h at 150 °C, and d) with the same sample as (c) under AM 1.5 light illumination.

gate voltage region. Robust adhesion of QDs to CNTs could enhance charge transfer, demonstrating a clear type conversion compared to loosely attached QDs shown in Figure 3b. This is evidence of electron charge transfer from QDs to CNTs, indicating type conversion by QD attachments, which has not been demonstrated previously. Another interesting phenomenon is the photo-quenching effect, where the source-drain current was reduced significantly upon AM 1.5 light illumination (Figure 3d). To examine this phenomenon further, QD+CNT sample was biased under light illumination and a reduction of I_{DS} was observed due to charge recombination. Electrons and holes are generated in QD upon light illumination.[3,4] Photogenerated holes could be transferred from QD to electron-rich CNT channel due to strong electrostatic interaction. As a consequence, the transferred holes could recombine with electrons in the CNT channel and the I_{DS} was suppressed to yield photo-quenching effect shown in Figure 3d. This photo-quenching effect in QD+CNT sample was in good contrast with positive photoconductance effect in QD+graphene system.[15] In the case of graphene, the gate bias was tuned to the intrinsic level so that electrons are excited near the Dirac point of metallic graphene, whereas in our case electrons are excited in p-type semiconducting CNT, therefore leading to impurity scattering which leads to negative photoconductivity.

The photo-quenching effect can be exploited in optical switch devices, where the current altered clearly (**Figure 4**) between the off-state (current decrease under light) and on-state (current increase in dark). The I_{DS} current flow through the QD+CNT channel under AM 1.5 light illumination was investigated at the off state (at −40 V gate bias, Figure 4a) and on state (at +40 V gate bias, Figure 4b) of the FET channel. Under light illumination, the I_{DS} current level decreased up to 600% at a negative gate bias and 250% at a positive gate bias, while removal of the light increased the current in the CNT channel back to the on state. This negative photoresponse behavior can be clearly verified by the demonstrated photo-quenching effect due to the photoexited charge transfer from QDs and subsequent charge recombination in SWCNT-FET channel. The remaining electrons in QDs (after each illumination cycle) could act as a local negative trap charges (local negative gate voltage) and suppress electron flow further in the CNT channel. This was manifested by the gradual reduction in the current level with repeated on/off light illumination (see green arrows). Photo-quenching efficiency (PQE) of the QD+CNT sample was calculated by the ratio between change in current due to light illumination and dark current, using equation $(I_{dark} - I_{light})/I_{dark} \times 100$, where I_{light} is the I_{DS} current under light illumination and I_{dark} is the dark current. Figure 4c represents the PQE variations of the QD+CNT sample under different source-drain and gate biasing conditions. Quenching efficiencies were similar to each other, independent of the gate bias but decreased significantly as the source-drain bias increased. The measured photo-quenching efficiency became highest at low source-drain bias (86.3% PQE at 0.5 V) and shows a lowest at high source-drain voltage (3.4% PQE at 4 V). Hot carriers at high applied electric field are less influenced by the variance of trap charge recombination in the

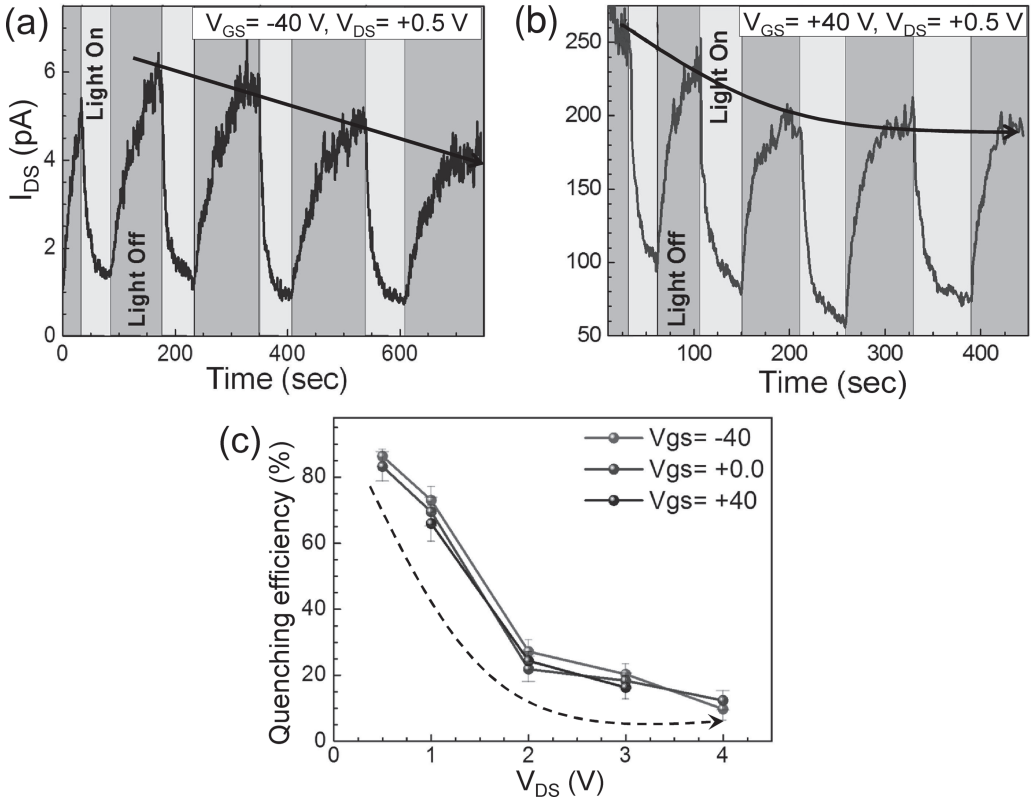

Figure 4. a) changes in I_{DS} due to light illumination (light on) and in the dark (light off) of the QD+SWCNT-FET (n-type) at a gate voltage (V_{GS}) of –40 V and a source drain voltage (V_{DS}) of +0.5 V. b) Under same conditions as (a), only V_{GS} was change to +40 V. c) Quenching efficiency variations with applied V_{DS} under three different fixed V_{GS} in QD+CNT sample. The PQE was calculated using the average current change due to light illumination from (a) and (b) and other applied voltages (not shown).

channel, resulting in low photo-quenching efficiency. This tunable PQE behavior with source-drain voltage could be advantageous and exploited in various photodetector applications in which photodetector efficiency have to be tuned well with external circuitry in order to exhibit required outputs.[11]

Attachment of QDs on highly efficient charge carriers of SWCNT facilitates efficient photogenerated charge collection from QDs, and moreover, the accumulated charges on SWCNT surface could enhance local electric field on QDs which could further enhance carrier-carrier interaction in QD systems. The presence of a strong external field from charged CNTs can invoke enhancement of temporal Stark effect in QDs themselves. The Stark effect has been observed in QDs due to quantum confinement effect on e–h pair wave function which is decoupled with decay time.[5–8] In general, the optical Stark effect can be monitored using PL spectroscopy.[8] Temporal PL peak shift and PL peak broadening were verified as the signature of optical stark effect in previous investigations.[7,8] **Figure 5**a,b show the time- resolved PL (TRPL) spectra from QD and QD+CNT samples, respectively. The PL peak positions were red-shifted and full width at half maximums (FWHMs) were broadened with time for QD samples, which is evidence of the optical Stark effect. Similar behavior was observed in QD+CNT samples but larger PL peak shift ($\Delta E \approx 88$ meV) and wider FWHM (ΔFWHM $\approx$ 65 meV) were observed compared to only QD case ($\Delta E \approx 74$ meV, ΔFWHM $\approx$ 32 meV). The presence of charged CNT can apply strong electrostatic field on the attached QD and could provoke stronger Stark effect. Figure 5c represents the temporal PL peak (main peak) shift extracted from the PL spectra in Figure 5a,b. The samples were excited in all of the TRPL measurements using a femtosecond pulse laser with a wavelength of 266 nm and a photon power density of 1 MW/cm^2. However, in confocal time-integrated PL (TIPL) measurements, a continuous wave laser (375 nm) with a photon power density of 15 W/cm^2 was used to excite the samples (Figure 2). Higher photon power density by 10^5 times and higher excitation energy by 1.35 eV in the TRPL investigations compared to TIPL resulted in blueshift and broadening in PL for both QD and QD+CNT samples in a similar manner.[34,35] PL peak shift difference between QD and QD+CNT samples was indistinguishable within 1 ns of photoexcitation (Figure 5c), indicating negligible charge transfer from QD to CNT. However, the PL peak shift became dominant in QD+CNT samples beyond 1 ns and showed a distinct region (marked by yellow background in Figure 5c) in which QD+CNT samples revealed a PL peak shift to long wavelength and more enhanced optical Stark effect compared with the QD samples. This large shift in QD+CNT samples is ascribed to the charge transfer from QD to CNT. In other words, the decoupling of e–h wavefunction is enhanced in QD+CNT sample by charge transfer. It should

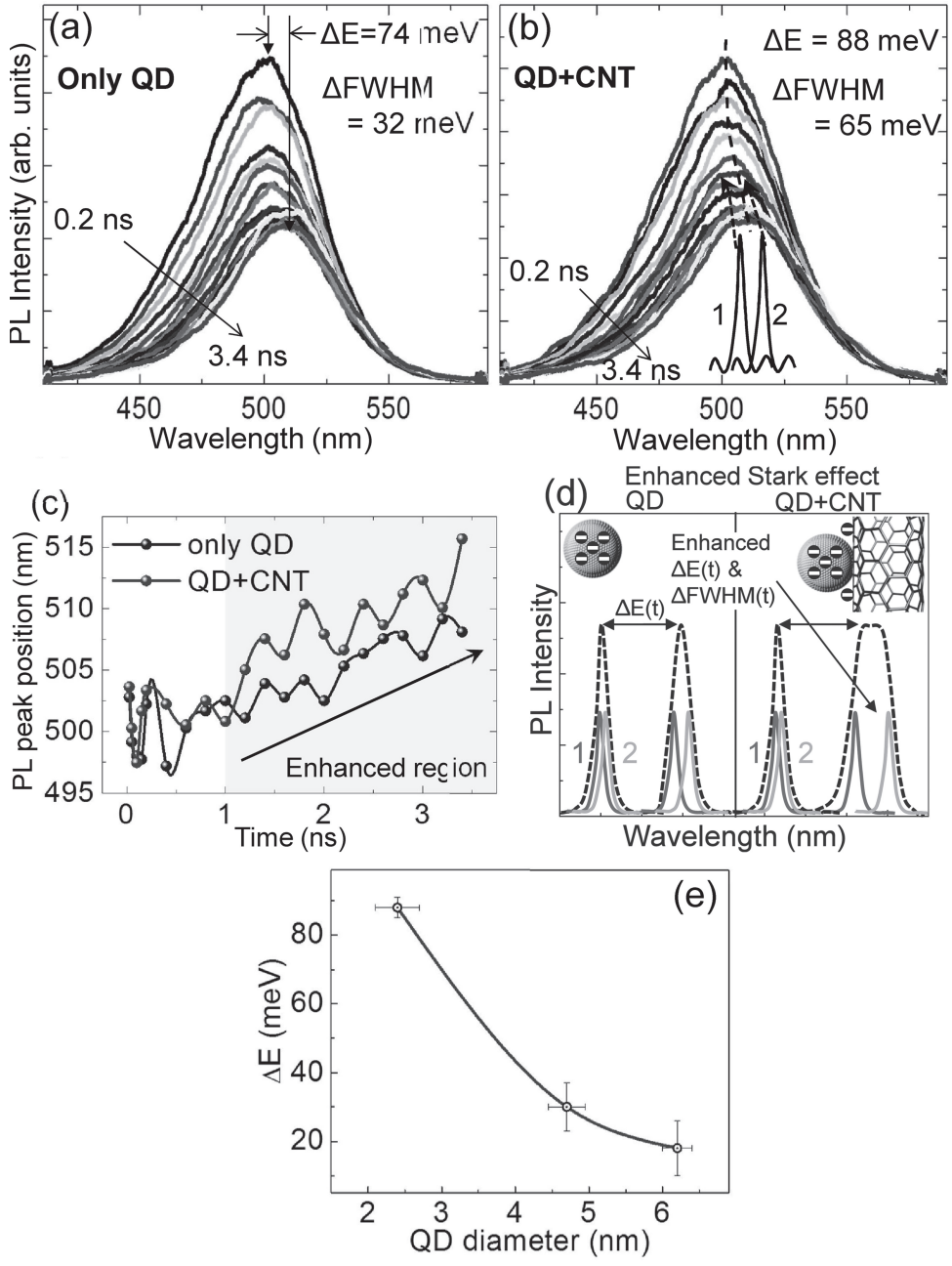

Figure 5. a,b) Temporal PL spectra in QD and QD+CNT samples with time in the range of ≈0.2–3.4 ns with a step of 0.2 ns. A femtosecond pulse laser (266 nm) was used for excitation. c) Temporal changes of PL peak (main peak) for QD and QD+CNT samples shown in (a) and (b). d) Schematic diagram of larger PL peak shift (energy shift Δ*E*) and peak broadening (ΔFWHM) in QD+CNT compared to QD case due to charged SWCNT. e) Δ*E* comparisons of our QD+CNT samples with SWCNT attached by larger diameter (4.7 nm and 6.2 nm) CdSe QDs.

be noted that these peaks were asymmetric particularly in both samples. The PL peak (defined as a main peak) can be split into two sub-peaks (peak 1 and peak 2) (indicated by dotted red arrow in Figure 5b).[7,8] The Stark effect from the PL spectrum was visualized in Figure 5d for both samples. The QD shows the temporal optical Stark effect due to decoupling of e–h wavefunction with time. However, the temporal peak shift is more prominent in QD+CNT with distinguishable peak broadening.[7,8] Temporal PL peak shift (Δ*E*) of QD+CNT sample was compared (Figure 5e) with larger diameter CdSe QDs attached to CNT surface. The PL peak shift was measured from 0.2 ns to 3.4 ns after excitation. The measured Δ*E* was reduced from 88 to 30 meV in 4.7 nm QDs and further reduced to 18 meV in 6.2 nm QDs. A larger diameter QD produces a smaller PL shift due to a reduced quantum confinement effect,[7,8] resulting in a reduced Stark effect.

To investigate this peak broadening effect due to charged CNTs, The PL peak was deconvoluted into two peaks due to inhomogeneous distribution of QD diameters:[7,8] a small-diameter QD peak (defined as Peak 1) and a large-diameter QD peak

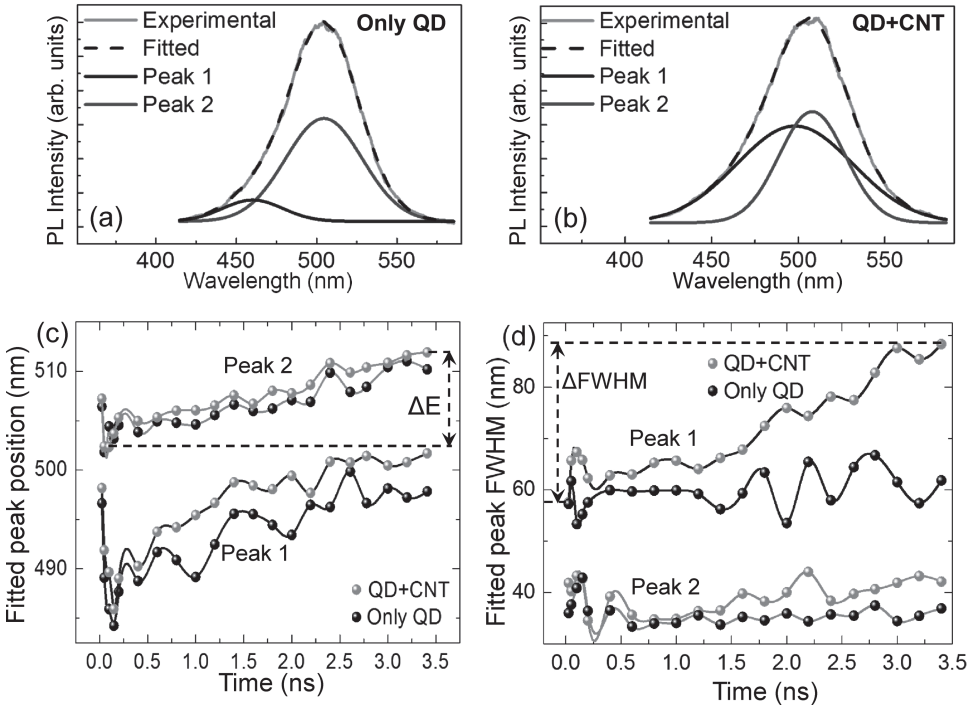

Figure 6. a,b) Measured PL spectrum collected between 1.6 ns to 1.8 ns after excitation from QD and QD+CNT samples was deconvoluted into superposition of two sub-peaks with Gaussian distributions: small-diameter QD (defined as Peak 1) and large-diameter QD (defined as Peak 2) peaks. c) Fitted PL peaks position change as a function of time. d) The fitted FWHM as a function of time.

Table 1. Stark shift comparison of QD and QD+CNT samples.

PL spectrum	ΔE [meV]		ΔFWHM [meV]	
	QD	QD+CNT	QD	QD+CNT
Main peak	74	88	32	65
Peak 1	70	80	56	150
Peak 2	40	39	17	43

(defined as Peak 2) (**Figure 6**a,b). A small portion of the small-diameter QDs was observed in QD sample. Peak 1 developed more prominently in QD+CNT due to an enhanced Stark effect in the small-diameter QDs. The shift in peak position and related FWHM reflects corroborated well the expected Stark effect, as shown in Figure 6c,d. Peak 2 is less affected by the presence of CNTs due to a reduced confinement effect in larger diameter QDs. This was evidenced by the smaller peak shift and FWHM in Peak 2, as shown in Figure 6c,d and summarized in **Table 1**.

3. Conclusions

Hybridization of the quantum dots to several nanostructures such as carbon nanotubes and nanowires involves complex charge transfer mechanisms. Negative photoresponse behavior in hybrid phototransistor of QDs/CNT driven by efficient charge collection mechanism with an enhanced optical Stark effect highlights the potential application of this device architecture in numerous optoelectronic devices. Tunable photoquenching efficiency in this hybrid device provides a chance to use a controlled photodetector matched with external circuitry in practical applications. Furthermore, these could be used for better understanding of quantum confined carrier dynamics in nanostructured systems. Our observations of an enhanced optical Stark effect have several implications. A strong external Coulomb force from charged SWCNTs could significantly amplify carrier multiplication effect in QDs. By designing smart QD+SWCNT hybrid structures, a highly efficient next generation solar cell could be fabricated, exploiting photoexited carrier extraction, an enhanced Stark effect, and the amplified carrier multiplication effect.

4. Experimental Section

Fabrication of SWCNT-FET: SWCNTs were synthesized on an array of catalyst photoresists (0.01 M of ferrocene) using a remote plasma-enhanced chemical vapor deposition (PECVD) system at low temperatures (450 °C). The CNT density was kept to be low to maintain a high on/off ratio in the FET. After synthesizing the SWCNTs on top of a 300 nm SiO_2/Si wafer, the corresponding source and drain electrodes (5 nm Ti/50 nm Au) were deposited using an electron beam evaporation system (A-tech system, Korea) to fabricate the CNT-FET.

Attachment of QDs on the SWCNT Surface: The CdSe-ZnS core-shell QDs functionalized with octadecylamine groups dispersed in toluene (QD+toluene) were purchased from Evident Technologies. The average outer QD diameter was 2.4 nm with 0.5 nm ZnS shell layer, corresponding to blue (2.5 eV) emission. The above SWCNT-FET device was immersed into QD+toluene solution and 1 V step potential was applied (from 1 to 6 V) between source-drain Ti/Au electrodes without gate biasing for

several minutes. After that the device was dried in vacuum for 2 h at 150 °C, followed by electrical and optical measurements.

Measurements: *I–V* characteristics of the SWCNT-FET were measured before and after QD attachment to the device. Furthermore, *I–V* characteristics of the device were evaluated under AM 1.5 light illumination (Solar light, model 16S-002-150-AM1.5). CdSe-ZnS core-shell QDs were attached to the surface of CNT by carboxyl surface functionalization for the transmission electron microscope measurements. Transmission electron microscopy of the QD-decorated carbon nanotube was performed using a JEOL JEM 2100F. The *I–V* characteristics of the CNT-TFTs were measured under ambient conditions by coupling two source-measure units (Keithley 6487). UV laser scanning confocal microscopy (Witec GmbH.) combined with a monochromator (30 cm, Acton) and a thermoelectric-cooled charge-coupled device detector (Princeton Instruments) was used to obtain the PL intensity plot and PL spectra of the samples. A continuous wave laser (375 nm) was used to excite the samples. Time-resolved PL (TRPL) spectroscopy of the samples was measured by using a streak camera (Hamamatsu, C4334) detector coupled with a monochromator. The sample was excited by a Ti:sapphire femtosecond pulse laser (Coherent, Mira 900) with a wavelength of 266 nm at 76 MHz with a 200 fs pulse width. All PL measurements were performed under ambient conditions.

Supporting Information

Supporting Information is available from the Wiley Online Library or from the author.

Acknowledgements

This work was partially supported by WCU program (R31-2008-000-10029-0) of the NRF of Korea funded by MEST and one of us (M.S.J.) acknowledges financial support by NANO R&D program (2007-02939) of the NRF of Korea funded by MEST. This work was also supported by the research center program of Institute for Basic Science.

Received: November 24, 2012
Revised: January 8, 2013
Published online: February 27, 2013

[1] A. P. Alivisatos, *Science* **1996**, *271*, 933–937.
[2] R. Schaller, V. Klimov, *Phys. Rev. Lett.* **2004**, *92*, 186601.
[3] R. D. Schaller, M. Sykora, S. Jeong, V. I. Klimov, *J. Phys. Chem. B* **2006**, *110*, 25332–25338.
[4] J. A. McGuire, J. Joo, J. M. Pietryga, R. D. Schaller, V. I. Klimov, *Acc. Chem. Res.* **2008**, *41*, 1810–1819.
[5] S. A. Empedocles, M. G. Bawendi, *Science* **1997**, *278*, 2114–2117.
[6] E. Menéndez-Proupin, C. Trallero-Giner, *Phys. Status Solidi C* **2004**, *1*, S42.
[7] S. A. Empedocles, R. Neuhauser, K. Shimizu, M. G. Bawendi, *Adv. Mater.* **1999**, *11*, 1243–1256.
[8] J. Müller, J. M. Lupton, A. L. Rogach, J. Feldmann, D. V. Talapin, H. Weller, *Phys. Rev. B* **2005**, *72*, 205339–205339.
[9] J. R. I. Lee, R. W. Meulenberg, K. M. Hanif, H. Mattoussi, J. E. Klepeis, L. J. Terminello, T. van Buuren, *Phys. Rev. Lett.* **2007**, *98*, 146803.
[10] R. W. Meulenberg, J. R. I. Lee, A. Wolcott, J. Z. Zhang, L. J. Terminello, T. van Buuren, *ACS Nano* **2009**, *3*, 325–330.
[11] A. N. Otte, J. Barral, B. Dolgoshein, J. Hose, S. Klemin, E. Lorenz, R. Mirzoyan, E. Popova, M. Teshima, *Nucl. Instrum. Methods Phys. Res., Sect. A* **2005**, *545*, 705–715.
[12] J. C. Carrano, D. J. H. Lambert, C. J. Eiting, C. J. Collins, T. Li, S. Wang, B. Yang, A. L. Beck, R. D. Dupuis, J. C. Campbell, *Appl. Phys. Lett.* **2000**, *76*, 924–926.
[13] A. J. Shields, M. P. O'Sullivan, I. Farrer, D. A. Ritchie, R. A. Hogg, M. L. Leadbeater, C. E. Norman, M. Pepper, *Appl. Phys. Lett.* **2000**, *76*, 3673–3675.
[14] L. Y. Leu, J. T. Gardner, S. R. Forrest, *J. Appl. Phys.* **1991**, *69*, 1052–1062.
[15] G. Konstantatos, M. Badioli, L. Gaudreau, J. Osmond, M. Bernechea, F. P. G. d. Arquer, F. Gatti, F. H. L. Koppens, *Nat. Nanotechnol.* **2012**, *7*, 363–368.
[16] A. Pandey, P. Guyot-Sionnest, *J. Phys. Chem. Lett.* **2009**, *1*, 45–47.
[17] M. Achermann, M. A. Petruska, S. A. Crooker, V. I. Klimov, *J. Phys. Chem. B* **2003**, *107*, 13782–13787.
[18] C. Biswas, Y. H. Lee, *Adv. Funct. Mater.* **2011**, *21*, 3806–3826.
[19] P. Avouris, Z. Chen, V. Perebeinos, *Nat. Nanotechnol.* **2007**, *2*, 605–615.
[20] C. Biswas, S. Y. Lee, T. H. Ly, A. Ghosh, Q. N. Dang, Y. H. Lee, *ACS Nano* **2011**, *5*, 9817–9823.
[21] K. I. Bolotin, K. J. Sikes, Z. Jiang, M. Klima, G. Fudenberg, J. Hone, P. Kim, H. L. Stormer, *Solid State Commun.* **2008**, *146*, 351–355.
[22] C. Biswas, F. Güneş, D. L. Duong, S. C. Lim, M. S. Jeong, D. Pribat, Y. H. Lee, *Nano Lett.* **2011**, *11*, 4682–4687.
[23] K. Yu, G. Lu, K. Chen, S. Mao, H. Kim, J. Chen, *Nanoscale* **2011**.
[24] B. H. Juárez, C. Klinke, A. Kornowski, H. Weller, *Nano Lett.* **2007**, *7*, 3564–3568.
[25] L. Hu, Y. L. Zhao, K. Ryu, C. Zhou, J. F. Stoddart, G. Grüner, *Adv. Mater.* **2008**, *20*, 939–946.
[26] S. Jeong, H. C. Shim, S. Kim, C.-S. Han, *ACS Nano* **2009**, *4*, 324–330.
[27] S. Y. Jeong, S. C. Lim, D. J. Bae, Y. H. Lee, H. J. Shin, S.-M. Yoon, J. Y. Choi, O. H. Cha, M. S. Jeong, D. Perello, M. Yun, *Appl. Phys. Lett.* **2008**, *92*, 243103.
[28] L. Brus, *Nano Lett.* **2010**, *10*, 363–365.
[29] S. Ritter, P. Gartner, N. Baer, F. Jahnke, *Phys. Rev. B* **2007**, *76*, 165302.
[30] S. A. Empedocles, M. G. Bawendi, *Science* **1997**, *278*, 2114–2117.
[31] C. Le Gall, A. Brunetti, H. Boukari, L. Besombes, *Phys. Rev. Lett.* **2011**, *107*, 057401.
[32] T. Unold, K. Mueller, C. Lienau, T. Elsaesser, A. D. Wieck, *Phys. Rev. Lett.* **2004**, *92*, 157401.
[33] A. Muller, W. Fang, J. Lawall, G. S. Solomon, *Phys. Rev. Lett.* **2009**, *103*, 217402.
[34] L. Van Dao, X. Wen, M. T. T. Do, P. Hannaford, E.-C. Cho, Y. H. Cho, Y. Huang, *J. Appl. Phys.* **2004**, *97*, 013501.
[35] B. Guo, Z. Ye, K. S. Wong, *J. Cryst. Growth* **2003**, *253*, 252–257.